Available online at www.sciencedirect.com
ScienceDirect
Nuclear Instruments and Methods in Physics Research B 261 (2007) 98–101
NIM B
Beam Interactions with Materials & Atoms
www.elsevier.com/locate/nimb

Production and application of a novel energy-tunable X-ray source at the RPI LINAC

Bryndol Sones [a], Yaron Danon [b,*], Robert Block [b]

[a] Department of Physics, United States Military Academy, ATTN: MADN-PHYS, 646 Swift Road, West Point, NY 10996-1905, United States
[b] Department of Mechanical, Aerospace and Nuclear Engineering, NES 1-9, Rensselaer Polytechnic Institute, 110 8th Street, Troy, NY 12180-3590, United States

Available online 28 March 2007

Abstract

The 60-MeV electron linear accelerator at Rensselaer Polytechnic Institute (RPI) is used to produce parametric X-rays (PXR). PXR is an intense, quasi-monochromatic, energy-tunable, and polarized X-ray source derived from the interaction of relativistic electrons with the periodic structure of crystal materials. Experiments were performed using highly oriented pyrolytic graphite (HOPG), LiF, Si, Ge, Cu, and W target crystal radiators. Smooth X-ray energy tunability is achieved by rotating the crystal with respect to the electron beam direction. Measured energy linewidths consistently agreed with predicted values except in cases using lower quality HOPG. When the predicted energy linewidth was narrower than our Si X-ray detector resolution (350 eV at 17.5 KeV), a near-absorption edge transmission technique that takes advantage of the PXR energy tunabilty was used to measure the PXR energy linewidth for example, Si(400) FWHM of 134 eV at 9.0 keV (2%). Per electron, the photon production efficiency of PXR is comparable to synchrotron radiation sources. A theoretical model that considers electron multiple scattering, electron divergence, and crystal mosaicity was used to broaden the PXR photon distribution in order to calculate the predicted PXR photon yield. Comparing measurements and calculations resulted in a typical relative error below 50%. In some cases with LiF, the differences between predicted and measured values were as low as 2% for LiF(400). Finally, this work reports for the first-time PXR imaging. This was achieved using LiF(220) interacting with 56 MeV electrons with electron beam currents up to 6 μA. The LiF and graphite PXR target crystals were compared for use in soft tissue imaging, e.g. mammography using energies 17–20 keV. Low Z materials like graphite and LiF were most suitable for PXR production because of their low Bremsstrahlung production, electron scattering, and photon absorption. Graphite was more efficient at producing PXR photons while the LiF energy line width was narrower.

PACS: 41.60.−m; 87.59.−e; 41.75.Fr

Keywords: Parametric X-rays; PXR; Crystal; Copper; Tungsten; Imaging; LINAC

1. Introduction

Parametric X-rays (PXR) are well known as an intense, tunable, quasi-monochromatic, and polarized X-ray source [1]. The production mechanism is the product of the interaction of relativistic electrons with a periodic medium or structure such as a single crystal. This novel radiation source is sometime described as the diffraction of ''virtual photons'' associated with relativistic electrons moving through a medium [2]. These virtual photons diffract from crystal planes in the same manner that Bragg's Law governs the diffraction of real photons. The first experimental realization of PXR occurred in 1985 [3], and since then both theoretical and experimental studies with electrons energies $E > 50$ MeV have distinguished PXR as having very high spectral intensity within a narrow angular and spectral range on the order of 10^{-3} [4,7]. In addition to Si as a PXR radiating crystal, PXR emitted from other

* Corresponding author. Tel.: +1 518 276 4008; fax: +1 518 276 4832.
E-mail address: danony@rpi.edu (Y. Danon).

0168-583X/$ - see front matter © 2007 Elsevier B.V. All rights reserved.
doi:10.1016/j.nimb.2007.03.034

crystals such as LiF, Ge, highly oriented pyrolytic graphite (HOPG), and W are reported [5–8]. Nonetheless, not until recently has an imaging application for PXR been demonstrated [9,10]. In early studies, electron beam currents were held to nA-levels to best characterize the PXR phenomenon [4]. Obstacles in demonstrating PXR imaging currently rests with the removal of crystal collision heating and the minimization of unwanted bremsstrahlung [11]. A method to overcome the bremsstrahlung obstacle is to use a low Z PXR target such as LiF or HOPG. Another method, the topic of this paper, is to examine a higher Z, metallic crystal.

2. Theory

Parametric X-rays are a continuously energy-tunable X-ray source whose photon energy is effectively independent of the incident electron energy and is determined solely by the spacing between crystal planes and by the experimental geometry. An expression for calculating the PXR energy is shown below in Eq. (1) [12].

$$E_{\mathrm{PXR}} = \hbar\omega_{\mathrm{PXR}} = \hbar c \frac{\tau \sin\phi}{1 - \cos\Omega}, \tag{1}$$

τ is the magnitude of the reciprocal lattice vector of the target crystallographic planes, ϕ is the electron incident angle measured with respect to the crystal planes, and Ω is the PXR emission angle measured with respect to the electron velocity. Bragg's Law is satisfied for the condition emission angle $\Omega = 2\phi$, which produces the maximum PXR intensity for a given electron incident angle. In the narrow cone of emitted PXR, the integrated PXR intensity is proportional to three important quantities shown in Eq. (2) [13,14].

$$N \propto f_{\mathrm{geo}} \chi^2 \mathrm{e}^{-2W}, \tag{2}$$

f_{geo} is a geometric factor which relates to the PXR escape path and absorption in the target crystal. Analysis of f_{geo} can be done to optimize the target crystal thickness for the maximum production of a given PXR energy; when maximized, the value for f_{geo} is equal to the absorption length, L_a, of the generated PXR energy in the crystal [11]. χ is the fourier component of the crystal's electric susceptibility for the given PXR energy. These two terms compete; in general, χ^2 increases with Z^2 while the L_a decreases with Z^4 [8]. Finally, e^{-2W} is the Debye–Waller factor which relates to the reduction of PXR production due to thermal lattice vibrations in the crystal. At room temperature, this factor is approximately equal to 1, and its reduction with increased crystal temperature depends on the Debye temperature and the lattice spacing. Crystals with lower Debye temperature, T_D, and smaller lattice spacing, d_{hkl}, are more affected by temperature increases.

For imaging applications, low Z target materials are attractive because compared to more dense metallic crystals, they minimize the production of unwanted Bremsstrahlung and crystal heating [5]. Still, the high susceptibilities of metallic crystals and their smaller optimized thickness can shed new light on their possible use in PXR imaging applications. Table 1 shows two important characteristics of PXR target crystals for a representative a 15 keV X-ray and 60 MeV electrons. The product $L_a\chi^2$ represents an idealized PXR production parameter and the last column represents the heating of a crystal with thickness L_a (for 15 keV X-rays) per μA of 60 MeV electrons. The use of thinner, metallic crystals produce less deposited heat on the target crystal. Of course, this heat is deposited on different crystal volumes, but how the crystal responds to the deposition of this heat is an important property in terms of the rugged survival of the crystal under the μA electron beam conditions needed for PXR imaging. In both experiments where PXR imaging is reported, the target crystals broke. At Rensselaer, the LiF crystal broke after multiple exposures of up to 30 s at 6 μA of 56 MeV electrons, and in Japan at Lebra, the Si crystal broke after exposure for unknown reported time intervals of 5 μA of 100 MeV electrons [15]. The temperature gradients in crystals that are locally heated by electron beam collisions can cause mechanically damaging stress–strain in the crystal and this heat must be dispersed via the conductivity of the crystal and other heat removal mechanisms such as forced convection [16]. By comparison, metal crystals are superior in thermal conduction; for example, Si and LiF have thermal conductivities of 2.3 and 12 W/(m °C), respectively, compared to 386 for Cu and 179 for W [17]. Other PXR studies have been done with W using highly relativistic electrons with energy of 500 MeV [8], and more recently, Cu has been investigated as a tunable X-ray source using non-relativistic electrons with an energy of 120 keV [4] and metallic polycrystals foils using a Mo and Si stack and moderately relativistic electrons with energy of 100 MeV have been reported [15]. This work reports PXR from Cu and W.

Table 1
Specific crystal plane characteristics, 15 keV PXR assumed for energy specific quantities and heating is for a crystal thickness of L_a

Crystal plane	L_a (μm)	χ_H (10^{-6})	$L_a\chi_H^2$ (μm 10^{-9})	T_D (K)	d (10^{-10} m)	Heating (mW/μA)
Be (002)	20759.0	1.300	35.1	1000	1.79	6400
Graphite (002)	9144.3	3.101	87.9	1860	3.35	2926
Diamond (111)	5849.5	2.368	32.8	1860	2.05	Unknown
LiF (200)	1568.8	2.768	12.0	730	2.01	722
LiF (220)	1568.8	1.978	6.1	730	1.42	722
Si (111)	443.7	2.271	2.3	625	3.14	195
Si (220)	443.7	2.601	3.0	625	1.92	195
Cu (111)	15.0	11.368	1.9	315	2.08	22
Ge (111)	20.5	5.183	0.6	360	3.27	17
W (110)	3.8	23.240	2.1	310	2.24	10
W (222)	3.8	18.940	1.4	310	0.91	10

3. Experimental setup

The general description of PXR experiments at RPI are discussed in earlier works [10]. In these experiments with

Cu and W, the crystals were both 1 mm thick and circular in shape with diameter of 1 cm double side polished 1 1 1 surface plane. PXR were produced using a Bragg geometry with an electron incident angle, ϕ, of approximately 30°, and PXR spectrum was measured by a well collimated Amptek, Si 25 mm^2 X-ray detector approximately 60° from the electron beam direction and 3 m away in air. The electron beam energy was 50 MeV and the beam current was kept to 200–600 of nA.

4. Results

The results shown in Figs. 1 and 2 demonstrate the first measurements of PXR from W and Cu at moderate relativistic electron energies. Data was collected for 4 min with linac electron beam currents of 200 nA for the W and 585 nA for Cu. Because the electron beam spot size is greater than the crystal itself and because of the rotation of the crystal with respects to the electron beam, the actual electron beam current incident of the crystals was estimated to be 12% of the machine current, or 24 nA for W and 70 nA for Cu. The florescence lines dominated the spectra for both W and Cu. Additionally, background under the measured peaks is relatively large and the bremsstrahlung continuum is easily observed. In typical PXR experiments, a rocking curve is often collected to optimize the PXR alignment and to investigate how the PXR intensity changes with crystal rotation about the Bragg angle. The spectra about the Bragg angle was not possible for W and was only limited with Cu because of the low signal to noise ratio and the sensitivity of the PXR detuning with these higher order reflections. In Fig. 1, there is an absence of a multiple of PXR for energies corresponding to W1 1 1 and W3 3 3 since these are forbidden reflections. The tungsten L florescence X-rays lines are clearly visible in the spectrum which also demonstrates a relatively large production of bremsstrahlung and large numbers of photons measured above 39 keV. Deadtime correction methods are employed using the procedures outline in our earlier work [18]. Like data in Fig. 1, the spectra for Cu shows K florescence X-rays lines and relatively large detected bremsstrahlung. Fig. 2 shows spectra for Cu 1 1 1 and higher multiples of this reflection. In this case, Cu1 1 1 is a permitted reflection but it is not observed since these X-rays with this energy (5.96 keV) are attenuated along the air pathway to the detector. The detected florescence X-rays should offer information about the electron beam current. A similar technique was used by Fiorito anf Rule when a Zr foil was added to the backside of the PXR crystal to check detector energy calibration and monitor relative electron beam current [19]. Using the PXR distribution broadening techniques developed by Potylitsin [20] and reported earlier from work at Rensselaer [21], the PXR yield when considering electron scattering in the target crystal and all other experimental parameters are consistent with the kinematical PXR theory. For Cu2 2 2 with an incident 70 nA beam current, the measured PXR yield was $2.6 \pm 0.5 \times 10^{-11}$ photons/e/9 mm^2 which is 30% larger than the theoretical calculation. For W2 2 2 with an incident 24 nA beam current, the measured PXR yield was $3.9 \pm 0.8 \times 10^{-11}$ photons/e/9 mm^2 which is 70% larger than the theoretical calculation.

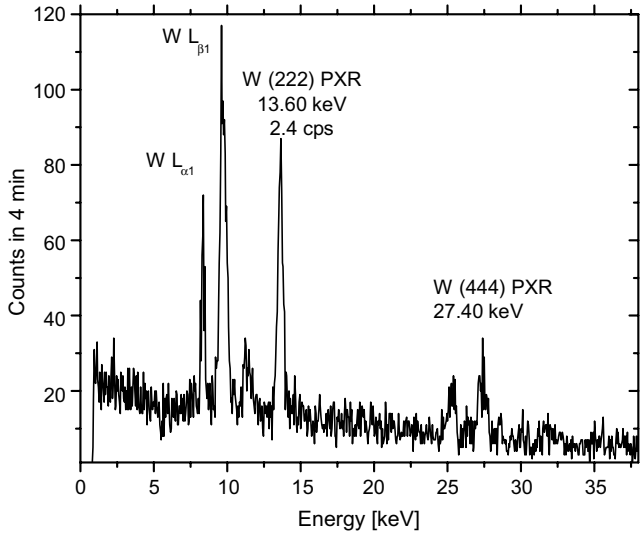

Fig. 1. Tungsten PXR spectrum showing W(2 2 2) and W(4 4 4) as well as more dominant L florescence lines, $\theta_B = 30°$. Electron beam current is 24 nA.

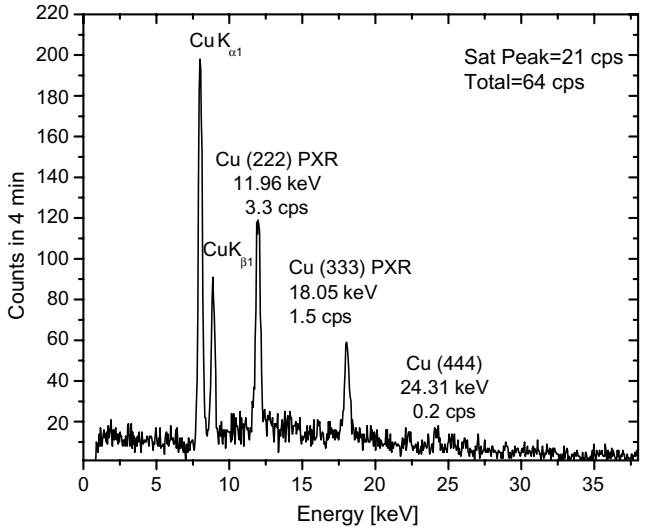

Fig. 2. Copper PXR spectrum showing Cu(2 2 2), Cu(3 3 3), Cu(4 4 4) as well as more dominant K florescence lines, $\theta_B = 30°$. Electron beam current is 70 nA.

5. Conclusions

Although higher Z target materials were once dismissed for PXR imaging applications, low Z crystals such as LiF and Si have been vulnerable to cracking when exposed to localized heating from electron beam currents in the μA level. Metallic crystals such as Cu and W produce PXR

spectra that are accompanied by florescence lines and relatively large amounts of bremsstrahlung. This work reports the production of PXR from Cu222 and W222 with reasonable agreement with theoretical predictions of PXR yield. However, the crystals used in this work are thicker than the optimum value reported in Table 1 which increased the observed bremsstrahlung. Future work includes heat modeling and heat dissipation using forced convection with liquid He and cooled air for both the metallic crystals and the low Z target crystals. Additional work is also necessary to analyze the material properties of these crystals and the stress–strain curves to identify crystal breaking conditions.

References

[1] P. Rulhusen, X. Artur, P. Dhez, in: World Scientific Series on Synchrotron Radiation Techniques and Applications, Vol. 4, 1998.
[2] M.L. Ter-Mikaelian, High Energy Electromagnetic Processes in Condensed Media, Wiley Interscience, New York, 1972.
[3] V.G. Baryshevshy, Phys. Lett. 110A (1985) 477.
[4] I.D. Feranchuk, K.G. Batrakov, Nucl. Instr. and Meth. A 543 (2005) 55.
[5] B. Sones, Y. Danon, R.C. Block, in: Fourth International Symposium on Radiation from Relativistic Electrons in Periodic Structures, Topical Issue, Nucl. Instr. Meth. B, 227, 2005, 22.
[6] A.V. Shchagin, V.I. Pritupa, N.A. Khizhnyak, Phys. Let. A 148 (1990) 485.
[7] E.A. Bogomazova, B.N. Kalinin, G.A. Naumenko, D.V. Padalko, A.P. Potylitsyn, A.F. Sharafutdinov, I.E. Vnukov, Nucl. Instr. and Meth. B 201 (2003) 276.
[8] Y. Adischev, S. Arishev, A. Vnukov, A. Yukolov, A. Polyitsyn, S. Kuznetsov, V. Zabaev, B. Kalinin, V. Kaplin, S. Uglov, A. Kubankin, N. Nasonov, Nucl. Instr. Meth. B 201 (2003) 114.
[9] Y. Hayakawa et. al., in: Present status of the parametric X-ray generator at LEBRA, Proceedings of the 1st annual meeting of the Particle Accelerator Society of Japan and the 29th Linear Accelerator Meeting in Japan, Aug 4-6, 2004 Funabashi Japan, access at www.linac.kek.jp/mirror/lam29.lebra.nihon-u.ac.jp/WebPublish/4B05.pdf.
[10] B. Sones, Y. Danon, R. Block, Nucl. Instr. and Meth. A 560 (2006) 589.
[11] B. Sones, Production of Intense, Tunable, Quasi-monochromatic X-rays Using the RPI Linear Accelerator, Ph.D. Dissertation, Rensselaer Polytechnic Institute, 2005.
[12] T. Akimoto, M. Tamura, J. Ikeda, Y. Aoki, F. Fujita, K. Sato, A. Honma, T. Sawamura, M. Narita, K. Imai, Nucl. Instr. and Meth. A 459 (2001) 78.
[13] K.H. Brenzinger et al., Phys. Rev. Lett. 79 (1997) 2462.
[14] J. Freudenberger, H. Genz, V. Morokhovshyi, A. Richter, J. Sellschop, Phys. Rev. Lett. 84 (2) (2000).
[15] Y. Takabayshi, I. Endo, K. Ueda, C. Moriyoshi, A.V. Shchagin, Nucl. Instr. and Meth. B 243 (2006) 453.
[16] S. Bellavia, S. Kahn, H. Kirk, H. Ludewig, D. Raparia, N. Simos, in: Proceedings of the 2005 Particle Accelerator conference, IEEE, Knoxville, Tn, 2005, p. 2209.
[17] L. Thomas, in: Heat Transfer, Professional Version, Capstone Publishing Corporation, Tulsa, OK, 1999.
[18] Y. Danon, B. Sones, R.C. Block, Nucl. Instr. and Meth. A 524 (2004) 287.
[19] R. Fiorito, D. Rule, in: Proceedings of the International Symposium of Radiation from Relativistic Electrons in Periodic Structures, September 4–8, 1995, Tomsk, Russia.
[20] A.P. Polylitsin, Influence of beam divergence and crystal mosaic structure upon parametric X-ray radiation characteristics. cond-mat/9802279, Vol. 1, 26 February, 1998.
[21] B. Sones, Y. Danon, R. Block, in: ANS Annual Meeting, San Diego CA, June 2005, p. 648.